High-Performance Fully Passive Discrete-State Continuous-Variable Quantum Key Distribution with Local Local Oscillator

Yu Zhang,[1] Xuyang Wang,[1,2,3,*] Chenyang Li,[4,†] Jie Yun,[1] Weilin Liu,[1] Qiang Zeng,[5] Zhiliang Yuan,[5] Zhenguo Lu,[1,2] and Yongmin Li[1,2,3,‡]

[1]State Key Laboratory of Quantum Optics Technologies and Devices, Institute of Opto-Electronics, Shanxi University, Taiyuan 030006, China
[2]Collaborative Innovation Center of Extreme Optics, Shanxi University, Taiyuan 030006, China
[3]Hefei National Laboratory, Hefei 230088, China
[4]Hong Kong Applied Science and Technology Research Institute, Hong Kong 999077, China
[5]Beijing Academy of Quantum Information Sciences, Beijing 100193, China

(Received 4 August 2025; revised 7 January 2026; accepted 27 March 2026; published 30 April 2026)

We propose and demonstrate a fully passive discrete-state continuous-variable quantum key distribution (CV-QKD), which can eliminate all modulator side channels on the source side, using a local local oscillator. Using specially designed phase rotation and discretization methods, the CV-QKD system achieves a maximum fiber transmission length of 100 km at a repetition rate of 1 GHz in asymptotic security, with the corresponding secret key bit rate being 70.7 kbps. In composable security, secret keys are distributed at 25 km of fiber with a secret key bit rate of 1.66 Mbps. Our protocol significantly simplifies the architecture of CV-QKD system by eliminating the need for optical modulators and random number generators as well as presents robust practical security and superior performance, which is comparable to that of its active discrete-state counterpart. Overall, this protocol is expected to play an important role in quantum metropolitan area networks and quantum access networks requiring high realistic security.

DOI: 10.1103/wgqv-cvr9

Introduction—Based on the fundamental laws of quantum mechanics, quantum key distribution (QKD) allows two distant parties to establish information-theoretically secure keys in the presence of eavesdroppers. The development of QKD has remarkably progressed since the BB84 protocol was proposed [1–5]. For discrete-variable (DV) QKD, the transmission length has been extended to 1200 km in free space [6], and to 1002 km in optical fibers [7]. For continuous-variable (CV) QKD, the transmission length has been extended to 202.81 km with transmitted local oscillator (TLO) [8], and to 100 km when using a local local oscillator (LLO) [9]. CV-QKD protocols are compatible with classical coherent optical communication, and the whole system can be integrated on a photonics chip [10–15]. They are promising to perform a crucial role in the quantum metropolitan area networks and quantum access networks [16–19].

When QKD protocols are implemented on realistic devices, side channels and device imperfections can compromise their security. Device-independent QKD protocol that guaranteed by the violation of the Bell inequality can promise the highest level of practical security [20–22]. However, the stringent requirements and low performance hinder its wide application. A more practical protocol, measurement-device-independent QKD, has been proposed and demonstrated to eliminate all side channels in the measurement devices [23–30]. Most state-of-the-art DV- and CV-QKD implementations assume trustworthy sources and perfectly prepared states [6–9]. However, realistic modulators can admit side channels that might directly leak information to an eavesdropper (Eve) and suffer from Trojan horse attacks [31–33]. In addition, perfect modulation in state preparation is prevented by many factors, such as the resolution of modulation [34], the stability of modulators [35], the correlations between adjacent pulses [36], the laser intensity fluctuation [37], and so on. Many effective methods have been proposed to solve the imperfections and quantify the potentially leaked information [38–45], but none can simultaneously handle all modulator side channels. A fully passive DV-QKD protocol has been proposed to eliminate modulator side channels at the source [46–49]. However, its secret key rate is at least an order of magnitude lower than that of its active counterpart. Thermal-source passive CV-QKD can achieve high-speed preparation of Gaussian states without active modulation [18,50–53]. However, it requires a high-power thermal source and mode overlap to suppress excess noise in passive-state preparation. Furthermore, photon-leakage noise due to the TLO scheme significantly limits

*Contact author: wangxuyang@sxu.edu.cn
†Contact author: chenyangli@astri.org
‡Contact author: yongmin@sxu.edu.cn

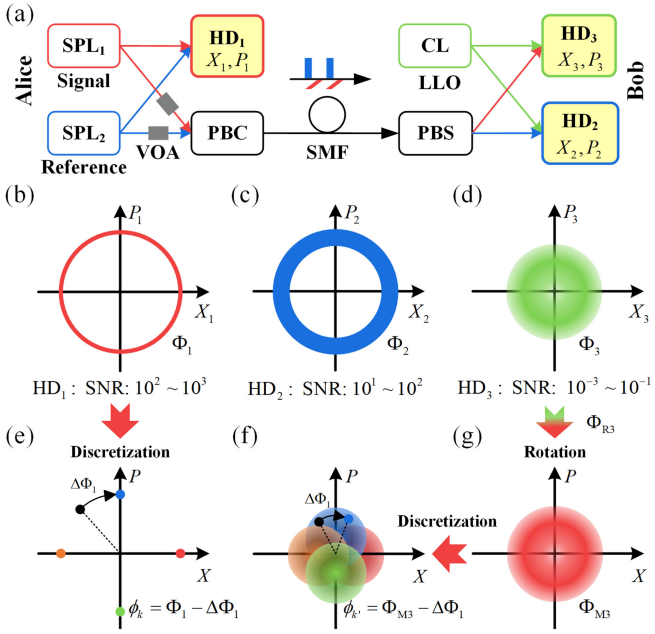

FIG. 1. Schematic of passive discrete-state LLO CV-QKD protocol and phase processing. (a) Schematic of the protocol; (b)–(d) Schematic of distribution of measurement data of three HDs in phase space; (e)–(g) Phase rotation and discretization. SPL: seeded pulse light; CL: continuous laser; VOA: variable optical attenuator; HD: heterodyne detection; PBC: polarization beam combiner; PBS: polarization beam splitter; SMF: single-mode fiber.

transmission lengths. Recently, passive discrete-state CV-QKD was developed to achieve secret key rates comparable to those under active CV-QKD while eliminating modulator-related side channels [54].

In this Letter, we propose and demonstrate a fully passive discrete-state LLO CV-QKD protocol. The transmitter (Alice) and receiver (Bob) obtain their data via the heterodyne detection of two phase-randomized and correlated pulsed light fields. By using phase rotation and discretization methods, discrete distribution of coherent states is achieved. As the protocol requires no active modulators and quantum random number generator, it greatly simplifies the CV-QKD system while showing performance comparable to those of active CV-QKD protocols [9,55–57]. Notably, the secret key rate is directly calculated based on the moments of quadratures or photon numbers at Bob's side by employing the semidefinite programming (SDP) method without any assumptions on the quantum channel.

Passive discrete-state LLO protocol—In the passive discrete-state LLO protocol as shown in Fig. 1(a), the transmitter Alice employs two independent seeded gained-switched lasers to generate two phase-randomized optical pulse sequences (one noted signal and the other noted reference), whose modes can be overlapped near perfectly [58–61]. Parts of signal and reference beams with high and equal intensities are injected into the heterodyne detector HD_1 to measure the quadratures of the signal (X_1, P_1) in a high signal to noise ratio (SNR). Alice attenuates the intensity of the other part of the signal beam to the single-photon level per pulse (quantum signal), and the other part of the reference beam to an appropriate level considering its influence on the quantum signal and the attenuation of the transmission channel. Both attenuated laser pulses are combined at a polarization beam combiner (PBC) and then sent to Bob via a single-mode fiber (SMF) in polarization and time multiplexing approach.

The receiver Bob demultiplexes the received reference and quantum signal pulses, and directs them into two heterodyne detectors (HD_2 and HD_3), respectively. In the heterodyne detection, both the reference and quantum signal pulses interfere with the continuous LLO beams from one laser, and the measured quadratures are (X_2, P_2) and (X_3, P_3), respectively. Figures 1(b)–1(d) depict the distribution of three kinds of measured states in the phase space. The typical range of HDs' SNRs are presented. A high SNR in HD_1 can ensure little prepared noise (see Sec. I of Supplemental Material [62]), and a high SNR in HD_2 enable the phase of the reference beam is determined.

Notice that Alice's gain-switched laser generates naturally phase-randomized states, whose phases are randomly distributed between 0 and 2π. Subsequently, by applying the floor function $\lfloor \Phi_1, (\pi/2) \rfloor = k$, $k = 0, 1, 2, 3$, and phase rotation of $\Delta\Phi_1 = \mathrm{mod}(\Phi_1, \pi/2)$, Alice transforms her initial phase-randomized states into random discrete states $|k\rangle$. The phase matching between Alice and Bob is accomplished through phase reference pulses, combined with blind phase searching using public quadrature data (detailed in the following section). Here, four-state discretization is shown as an example. Other numbers of discretization are straightforward.

The subsequent parameter estimation process is similar to that of the prepare-and-measure scheme in discrete-modulation protocols [70]. Alice publicly announces the amplitude of the prepared states, then Bob estimates the system parameters and calculates the secret key rates using Eqs. (1) and (2). Under linear-channel assumption, the channel transmission T and excess noise ε are usually estimated to calculate the secret key rate [37]. Herein, the moments estimated on Bob's side are directly employed as constrained conditions to calculate the secret key rate. In asymptotic security, the first- and second-order moments of quadratures are used as the constraint conditions; while in composable security, the constraint conditions are the first- and second-order moments of photon numbers. In these cases, there are not any assumptions about the quantum channel, and there is also no need to estimate the excess noise on Alice's side.

The asymptotic secret key rate in reverse reconciliation is given by [63,71]:

$$R^{\infty} = \min_{\rho_{\mathrm{AB}} \in \mathcal{S}} f(\rho_{\mathrm{AB}}) - p_{\mathrm{pass}} \delta_{\mathrm{EC}}. \tag{1}$$

The set $\mathcal{S}$ contains all density operators ρ_{AB} compatible with experimental observations, where ρ_{AB} is the joint state

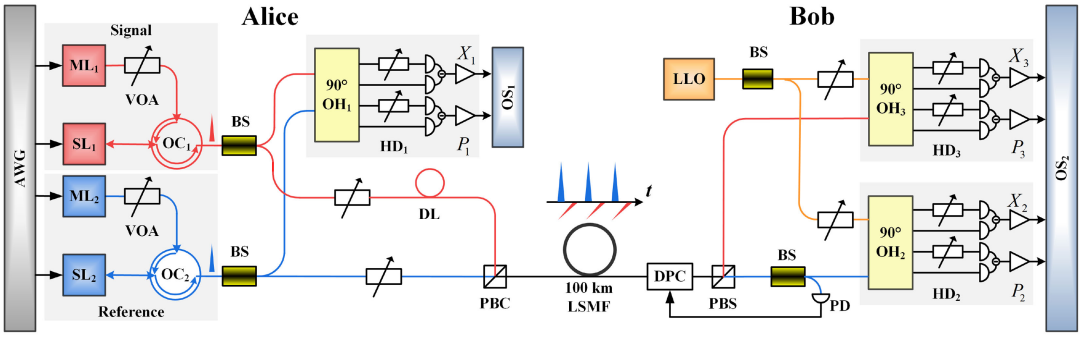

FIG. 2. Schematic of the experimental setup. AWG: arbitrary waveform generator; ML: master laser; SL: slave laser; OC: optical circulator; BS: beam splitter; OH: optical hybrid; DL: delay line; DPC: dynamic polarization controller; PD: photodetector; LLO: local local oscillator; LSMF: low-loss single-mode fiber; OS: oscilloscope.

of Alice and Bob. The function $f(\rho_{AB}) = D[\mathcal{G}(\rho_{AB})\|\mathcal{Z}(\mathcal{G}(\rho_{AB}))]$ is the quantum relative entropy, and its minimum value can be optimized using the SDP. The parameter p_{pass} represents the sifting probability. The term δ_{EC} is the information leaked during the error-correction step.

The secret key rate in composable security in reverse reconciliation is [72]

$$R \leq \frac{n}{N}\left[\min_{\rho_{AB}\in\mathcal{S}} f(\rho_{AB}) - \delta(\bar{\epsilon}) - \Delta(w)\right] - \delta_{leak}^{EC} - \delta(\epsilon_{PA}), \quad (2)$$

where $\delta(\bar{\epsilon}) = 2\log_2(\mathrm{rank}(\rho_A)+3)\sqrt{\log_2(2/\bar{\epsilon})/n}$, $\bar{\epsilon}$ is the security parameter for smoothing, $\Delta(w)$ is the determined correction term, $\delta(\epsilon_{PA}) = 2\cdot\log_2(1/\epsilon_{PA})/N$, and ϵ_{PA} is the security parameter for privacy amplification (see Sec. II of Supplemental Material for details [62]).

The subsequent steps of the protocol follow the key map and the standard data postprocessing procedures, including reverse reconciliation and privacy amplification [64,65,73,74].

Experimental setup—Figure 2 illustrates the experimental setup of fully passive discrete-state LLO CV-QKD. Both the seeded pulse laser sources on Alice's side comprise a gain-switched master laser (ML), a variable optical attenuator (VOA), an optical circulator (OC), and a gain-switched slave laser (SL). A four-channel arbitrary waveform generator (AWG) is employed to drive the lasers to generate two synchronous pulse sequences with a repetition rate of 1 GHz. The widths of the electrical pulses used to drive the ML and SL are 300 and 200 ps, respectively. The intensities of laser pulses injected into and output from the SL are $\sim 10^6$ and $\sim 10^7$ photons per pulse. This method can reduce the emission time jitter and enable frequency chirp synchronization while maintaining random phases of the emitted laser pulses. The center wavelength of all lasers was tuned to 1550.12 nm using temperature controllers. The observed second-order intensity correlation value of interference between the signal and reference pulses is $g^{(2)} = 1.47$, almost reaching the theoretical limit of 1.50 [58].

The intensities of the signal and reference pulses incident on HD_1 are both $\sim 10^6$ photons per pulse. The output paths of the 90° optical hybrid (OH) are equipped with two VOAs to balance the two arms of the balanced photoreceivers. The measurement results were acquired by a high-speed oscilloscope (OS_1). At the input ports of the PBC, the intensities of quantum signal pulses and reference pulses are ~ 1 and $\sim 10^4$–10^6 photons per pulse, respectively.

At the receiver side, Bob demultiplexes the quantum signal and reference pulses using a dynamic polarization controller (DPC), a polarization beam splitter (PBS), a beam splitter (BS), and a photodetector (PD). To measure the quadratures of the quantum signal and reference pulses, a continuous laser with a center wavelength of 1550.12 nm was used as LLO. During the quantum signal transmission, the laser pulses were sent by frame, which contains 10^7 pulses. All output signals of the HDs were sampled using high-speed OS_2.

System performance was demonstrated on four transmission fibers with different lengths (0 km/back to back, 25 km, 50 km, and 100 km) in asymptotic security. In the case of the 0 km fiber, the transmitter and receiver were directly connected to calibrate the amplitude of the prepared states and achieve the maximum secret key rate. The 25 and 50 km fibers were standard SMFs, whereas the 100 km fiber is a low-loss SMF (0.16 dB/km). System performance considering composable security was evaluated at 25 km, and the secret keys were achieved using reverse reconciliation and privacy amplification (Sec. III of Supplemental Material [62]).

Phase rotation and discretization—In heterodyne detection, the relative phase of each light pulse can be determined by its quadratures X and P. The relative phases measured by three HDs are

$$\begin{aligned} HD_1 &: \Phi_1 = \varphi_S - \varphi_R + \theta_{S1}, \\ HD_2 &: \Phi_2 = \varphi_R - \varphi_L + \theta_{F2} + \theta_{S2}, \\ HD_3 &: \Phi_3 = \varphi_S - \varphi_L + \theta_{F3} + \theta_{S3} + \Delta\theta, \end{aligned} \quad (3)$$

where φ_S, φ_R, and φ_L are the initial phases of the signal, reference, and LLO beams, respectively, and φ_S, φ_R are

independently and randomly distributed in $[0, 2\pi)$ for each pulse. As the linewidth of the LLO beam is of the order of megahertz, and the laser pulse width is 200 ps, φ_L can be treated as a constant value within each pulse. The slow-drift phases θ_{S1}, θ_{S2}, and θ_{S3} arise from the optical path difference of the tens of meters fiber, and the corresponding drift speed is ~100 rad/s. The fast-drift phases θ_{F2} and θ_{F3}, which are caused by the same long SMF, are equal and the drift speeds are ~krad/s at 100 km. Due to low SNR for the quantum signal, the effect of the shot noise on the relative phase Φ_3 cannot be neglected and is denoted as $\Delta\theta$.

To align the relative phases between Alice and Bob by block, which contains 10^5 pulses in a 100 μs duration, Bob rotates Φ_3 according to Φ_2 to eliminate the relative phases φ_L, θ_{F2} and θ_{F3}. This rotation yields

$$\Phi_{R3} = \Phi_3 - \Phi_2 = \varphi_S - \varphi_R + \theta_{S32} + \Delta\theta, \tag{4}$$

where $\theta_{S32} = \theta_{S3} - \theta_{S2}$.

Alice's phases Φ_1 and Bob's phases Φ_{R3} are correlated due to the same component of $\varphi_S - \varphi_R$. The correlation value is degraded by the noise terms θ_{S1}, θ_{S32}, and $\Delta\theta$. The slow-drift phases θ_{S1} and θ_{S32} can be treated as constant values in each block. In the aligning process, 10% of the pulses within the blocks are consumed. Alice declares her pulses' phases set $\{\Phi_1\}$ to Bob. Then Bob adds scanning phase θ_{scan} to the corresponding phases set $\{\Phi_{R3}\}$ to generate $\{\Phi'_{R3}\} = \{\Phi_{R3}\} + \theta_{scan}$, and determine the correlation coefficients of the cosine values of the phases set $\{\Phi'_{R3}\}$ and the set $\{\Phi_1\}$. The scanning phase that corresponds to the maximum correlation is noted as the compensation phase θ_{max}. In this case, the relationship of θ_{max}, θ_{S1}, and θ_{S32} is $\theta_{S1} = \theta_{S32} + \theta_{max}$. Then, Bob rotates his remaining phases with θ_{max} to achieve maximally correlated phases $\Phi_{M3} = \Phi_{R3} + \theta_{max} = \Phi_1 + \Delta\theta$. Through above phase rotation operation, Alice's phases Φ_1 [Fig. 1(b)] and Bob's phases Φ_{M3} [Fig. 1(g)] are aligned. Additional details about phase drift and scanning are provided in Sec. IV of Supplemental Material [62].

In phase discretization stage, Alice transforms the phase Φ_1 in each block using the following criteria and announces publicly the phases $\Delta\Phi_1$:

$$\left\lfloor \Phi_1, \frac{\pi}{2} \right\rfloor = k, \quad k = (0, 1, 2, 3), \quad \mathrm{mod}\left(\Phi_1, \frac{\pi}{2}\right) = \Delta\Phi_1. \tag{5}$$

After rotating Φ_1 by angle $\Delta\Phi_1$, all of Alice's quadratures are discretized to four kinds of points corresponding to four kinds of phases $\phi_k = \Phi_1 - \Delta\Phi_1 = k\pi/2$ or prepared signal states $|k\rangle$ [Fig. 1(e)]. For example, the quadratures of one pulse before discretization $X_1 + iP_1 = |X_1 + iP_1|e^{i\Phi_1}$ and after discretization $|X_1 + iP_1|e^{i\phi_k}(k = 1)$ are drawn as the black and blue points, respectively, in Fig. 1(e). Subsequently, Bob rotates Φ_{M3} by $\Delta\Phi_1$ so as to obtain $\phi_{k'} = \Phi_{M3} - \Delta\Phi_1$, in the same way as Alice did. All of his quadratures are then discretized to four kinds of circles or discrete displaced thermal states, shown in Fig. 1(f). His raw key string follows the key map:

$$k' = j, \quad \text{if } \phi_{k'} \in \left[\frac{(2j-1)\pi}{4}, \frac{(2j+1)\pi}{4}\right), \tag{6}$$

where $j = (0, 1, 2, 3)$. At this stage, Alice and Bob share correlated raw key string (k, k').

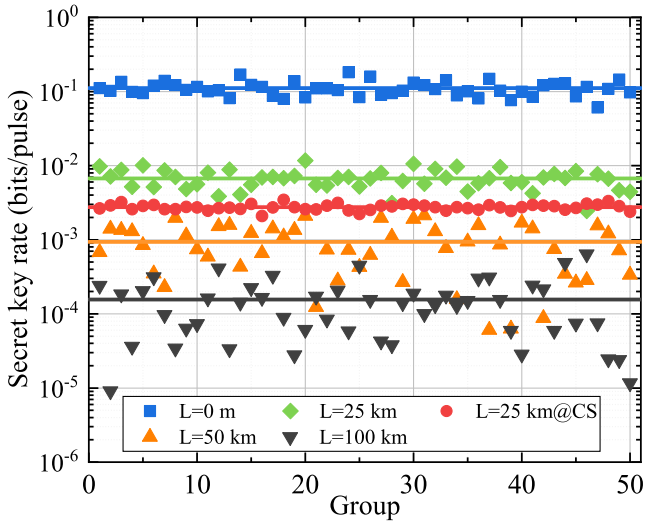

FIG. 3. Secret key rates: at 0 (blue squares), 25 (green diamonds), 50 (orange upright triangles), and 100 (black inverted triangles) km in asymptotic security; 25 km (red dots) in composable security. The lines represent the average values of the corresponding secret key rates.

Experimental results—The asymptotic secret key rates R at four different transmission lengths and the secret key rate in composable security at 25 km are presented in Fig. 3. The secret key rates were estimated for 50 groups of raw keys for each situation, and the corresponding average values were plotted (solid lines). System parameters and secret key rates at different transmission lengths are shown in Table I. When the transmission length is longer, more quantum signal pulses are required to maintain a sufficiently high success rate η_S.

To evaluate the performance of our experimental system, the estimated excess noises ε_E are listed when a linear quantum channel is assumed (Sec. V of Supplemental Material [62]). The secret key bit rate is defined by $K = R \cdot N_{eff} \cdot (1 - \eta_{FER})$, where N_{eff} represents the number of quantum signal pulses used to extract the secret key per second.

At transmission length of 100 km, the asymptotic secret key bit rate is 70.7 kbps. By considering the composable security and implementing the information reconciliation and privacy amplification, a secret key bit rate of 1.66 Mbps is achieved. Detailed performance comparison between our system and the existing systems can be seen in Sec. VI of Supplemental Material [62]. We see that the performance of

TABLE I. System parameters at different transmission lengths L. CS: composable security; N: amount of quantum signal pulses in a group; η_S: success rate in estimating secret key rate; $|\alpha|$: amplitude of quantum signal; η_{RR}: reverse reconciliation efficiency; η_{FER}: frame error rate; R: secret key rate; K: secret key bit rate; bpp: bits per pulse; bps: bits per second; SNU: shot noise unit; electronic noise: $V_{el} = 0.189$ SNU; detection efficiency: $\eta = 0.352$.

L	0 km	25 km		50 km		100 km	25 km in CS
N	10^8	10^8	10^9	10^9	10^{10}	10^{10}	10^{10}
η_S	100%	90%	100%	92%	96%	82%	100%
$\lvert\alpha\rvert(\sqrt{\text{SNU}})$	1.15	0.821		0.773		0.753	0.785
$\varepsilon_E(\text{SNU})$	0.0239	0.0281		0.0291		0.0262	0.0257
η_{RR}	0.95	0.95		0.95		0.95	0.951
η_{FER}	0.10	0.27		0.30		0.50	0.326
$\langle R\rangle$ (bpp)	1.1×10^{-1}	6.7×10^{-3}		9.3×10^{-4}		1.6×10^{-4}	2.7×10^{-3}
K (Mbps)	89.9	4.42		0.588		0.0707	1.66

our system is comparable to the active discrete-modulation CV-QKD protocol [55,56,66–68].

Conclusions and outlook—We propose and demonstrate a high-performance fully passive discrete-state LLO CV-QKD protocol that eliminates all modulator side channels on the source side. Leveraging seeded, gain-switched pulsed laser sources alongside dedicated phase rotation and discretization techniques, this system achieves secret key bit rates of 1.66 Mbps at 25 km (composable security) and 70.7 kbps at 100 km (asymptotic security). Through SDP, the secret key rate can be calculated directly using constrained moments, eliminating the need to estimate the excess noise or impose linear assumption on the quantum channel.

In the future, we will increase the system repetition rate to above 10 GHz considering that pulse width can be reduced to ~20 ps [58]. The reverse reconciliation at longer distance ($\geq$ 25 km) will be explored. Furthermore, the present four states protocol can be extended to eight or more discrete states protocol to improve the system performance.

Acknowledgments—This work was supported in part by the National Natural Science Foundation of China under Grants No. 11504219, No. 62175138, No. 62205188, and No. 11904219, and in part by the Quantum Science and Technology-National Science and Technology Major Project under Grant No. 2021ZD0300703.

Data availability—The data that support the findings of this article are not publicly available upon publication because it is not technically feasible and/or the cost of preparing, depositing, and hosting the data would be prohibitive within the terms of this research project. The data are available from the authors upon reasonable request.

[1] F. Xu, X. Ma, Q. Zhang, H.-K. Lo, and J.-W. Pan, Rev. Mod. Phys. **92**, 025002 (2020).
[2] Y. C. Zhang, Y. M. Bian, Z. Y. Li, S. Yu, and H. Guo, Appl. Phys. Rev. **11**, 011318 (2024).
[3] S. Pirandola, U. L. Andersen, L. Banchi, M. Berta, D. Bunandar, R. Colbeck, D. Englund, T. Gehring, C. Lupo, C. Ottaviani *et al.*, Adv. Opt. Photonics **12**, 1012 (2020).
[4] C. Weedbrook, S. Pirandola, R. García-Patrón, N. J. Cerf, T. C. Ralph, J. H. Shapiro, and S. Lloyd, Rev. Mod. Phys. **84**, 621 (2012).
[5] V. Scarani, H. Bechmann-Pasquinucci, N. J. Cerf, M. Dušek, N. Lütkenhaus, and M. Peev, Rev. Mod. Phys. **81**, 1301 (2009).
[6] S. K. Liao, W. Q. Cai, W. Y. Liu, L. Zhang, Y. Li, J. G. Ren, J. Yin, Q. Shen, Y. Cao, Z. P. Li *et al.*, Nature (London) **549**, 43 (2017).
[7] Y. Liu, W. J. Zhang, C. Jiang, J. P. Chen, C. Zhang, W. X. Pan, D. Ma, H. Dong, J. M. Xiong, C. J. Zhang *et al.*, Phys. Rev. Lett. **130**, 210801 (2023).
[8] Y. C. Zhang, Z. Y. Chen, S. Pirandola, X. Y. Wang, C. Zhou, B. J. Chu, Y. J. Zhao, B. J. Xu, S. Yu, and H. Guo, Phys. Rev. Lett. **125**, 010502 (2020).
[9] A. A. E. Hajomer, I. Derkach, N. Jain, H. M. Chin, U. L. Andersen, and T. Gehring, Sci. Adv. **10**, eadi9474 (2024).
[10] G. Zhang, J. Y. Haw, H. Cai, F. Xu, S. M. Assad, J. F. Fitzsimons, X. Zhou, Y. Zhang, S. Yu, J. Wu *et al.*, Nat. Photonics **13**, 839 (2019).
[11] L. Li, T. Wang, X. H. Li, P. Huang, Y. Y. Guo, L. J. Lu, L. J. Zhou, and G. H. Zeng, Photonics Res. **11**, 504 (2023).
[12] Y. X. Jia, X. Y. Wang, X. Hu, X. Hua, Y. Zhang, X. B. Guo, S. X. Zhang, X. Xiao, S. H. Yu, J. Zou *et al.*, New J. Phys. **25**, 103030 (2023).
[13] Y. M. Bian, Y. Pan, X. S. Xu, L. Zhao, Y. Li, W. Huang, L. Zhang, S. Yu, Y. C. Zhang, and B. J. Xu, Appl. Phys. Lett. **124**, 174001 (2024).
[14] Y. Piétri, L. T. Vidarte, M. Schiavon, L. Vivien, P. Grangier, A. Rhouni, and E. Diamanti, Opt. Quantum **2**, 428 (2024).
[15] A. A. E. Hajomer, C. Bruynsteen, I. Derkach, N. Jain, A. Bomhals, S. Bastiaens, U. L. Andersen, X. Yin, and T. Gehring, Optica **11**, 1197 (2024).
[16] Y. D. Huang, T. Shen, X. Y. Wang, Z. Y. Chen, B. J. Xu, S. Yu, and H. Guo, Phys. Rev. Appl. **16**, 064051 (2021).
[17] X. Y. Wang, Z. Y. Chen, Z. H. Li, D. K. Qi, S. Yu, and H. Guo, Opt. Lett. **48**, 3327 (2023).
[18] F. Y. Ji, P. Huang, T. Wang, X. Q. Jiang, and G. H. Zeng, Photonics Res. **12**, 1485 (2024).

[19] A. A. E. Hajomer, I. Derkach, R. Filip, U. L. Andersen, V. C. Usenko, and T. Gehring, Light Sci. Appl. **13**, 291 (2024).

[20] W. Zhang, T. van Leent, K. Redeker, R. Garthoff, R. Schwonnek, F. Fertig, S. Eppelt, W. Rosenfeld, V. Scarani, C. C.-W. Lim *et al.*, Nature (London) **607**, 687 (2022).

[21] L. Wooltorton, P. Brown, and R. Colbeck, Phys. Rev. Lett. **132**, 210802 (2024).

[22] E. Y.-Z. Tan and R. Wolf, Phys. Rev. Lett. **133**, 120803 (2024).

[23] H.-K. Lo, M. Curty, and B. Qi, Phys. Rev. Lett. **108**, 130503 (2012).

[24] S. L. Braunstein and S. Pirandola, Phys. Rev. Lett. **108**, 130502 (2012).

[25] Y. Liu, T. Y. Chen, L. J. Wang, H. Liang, G. L. Shentu, J. Wang, K. Cui, H. L. Yin, N. L. Liu, L. Li, X. Ma, J. S. Pelc, M. M. Fejer, C. Z. Peng, Q. Zhang, and J. W. Pan, Phys. Rev. Lett. **111**, 130502 (2013).

[26] H. L. Yin, T. Y. Chen, Z. W. Yu, H. Liu, L. X. You, Y. H. Zhou, S. J. Chen, Y. Mao, M. Q. Huang, W. J. Zhang, H. Chen, M. J. Li, D. Nolan, F. Zhou, X. Jiang, Z. Wang, Q. Zhang, X. B. Wang, and J. W. Pan, Phys. Rev. Lett. **117**, 190501 (2016).

[27] Y. Cao, Y. H. Li, K. X. Yang, Y. F. Jiang, S. L. Li, X. L. Hu, M. Abulizi, C. L. Li, W. Zhang, Q. C. Sun *et al.*, Phys. Rev. Lett. **125**, 260503 (2020).

[28] Y. H. Li, S. L. Li, X. L. Hu, C. Jiang, Z. W. Yu, W. Li, W. Y. Liu, S. K. Liao, J. G. Ren, H. Li *et al.*, Phys. Rev. Lett. **131**, 100802 (2023).

[29] Y. Tian, P. Wang, J. Q. Liu, S. N. Du, W. Y. Liu, Z. G. Lu, X. Y. Wang, and Y. M. Li, Optica **9**, 492 (2022).

[30] S. Pirandola, C. Ottaviani, G. Spedalieri, C. Weedbrook, S. L. Braunstein, S. Lloyd, T. Gehring, C. S. Jacobsen, and U. L. Andersen, Nat. Photonics **9**, 397 (2015).

[31] N. Gisin, S. Fasel, B. Kraus, H. Zbinden, and G. Ribordy, Phys. Rev. A **73**, 022320 (2006).

[32] N. Jain, E. Anisimova, I. Khan, V. Makarov, C. Marquardt, and G. Leuchs, New J. Phys. **16**, 123030 (2014).

[33] A. Gnanapandithan, L. Qian, and H.-K. Lo, Phys. Rev. Lett. **134**, 130802 (2025).

[34] P. Jouguet, S. Kunz-Jacques, E. Diamanti, and A. Leverrier, Phys. Rev. A **86**, 032309 (2012).

[35] W. Y. Liu, X. Y. Wang, N. Wang, S. N. Du, and Y. M. Li, Phys. Rev. A **96**, 042312 (2017).

[36] K. I. Yoshino, M. Fujiwara, K. Nakata, T. Sumiya, T. Sasaki, M. Takeoka, M. Sasaki, A. Tajima, M. Koashi, and A. Tomita, npj Quantum Inf. **4**, 8 (2018).

[37] F. Laudenbach, C. Pacher, C.-H. F. Fung, A. Poppe, M. Peev, B. Schrenk, M. Hentschel, P. Walther, and H. Hübel, Adv. Quantum Technol. **1**, 1800011 (2018).

[38] C. Y. Li, L. Qian, and H.-K. Lo, npj Quantum Inf. **7**, 150 (2021).

[39] D. Huang, P. Huang, D. k. Lin, and G. H. Zeng, Sci. Rep. **6**, 19201 (2016).

[40] I. Derkach, V. C. Usenko, and R. Filip, Phys. Rev. A **96**, 062309 (2017).

[41] V. C. Usenko and R. Filip, Phys. Rev. A **81**, 022318 (2010).

[42] I. Derkach, V. C. Usenko, and R. Filip, Phys. Rev. A **93**, 032309 (2016).

[43] K. Tamaki, M. Curty, and M. Lucamarini, New J. Phys. **18**, 065008 (2016).

[44] M. Pereira, M. Curty, and K. Tamaki, npj Quantum Inf. **5**, 62 (2019).

[45] A. A. E. Hajomer, N. Jain, H. Mani, H.-M. Chin, U. L. Andersen, and T. Gehring, npj Quantum Inf. **8**, 136 (2022).

[46] W. Wang, R. Wang, C. Q. Hu, V. Zapatero, L. Qian, B. Qi, M. Curty, and H.-K. Lo, Phys. Rev. Lett. **130**, 220801 (2023).

[47] F. Y. Lu, Z. H. Wang, V. Zapatero, J. L. Chen, S. Wang, Z. Q. Yin, M. Curty, D. Y. He, R. Wang, W. Chen *et al.*, Phys. Rev. Lett. **131**, 110802 (2023).

[48] C. Q. Hu, W. Y. Wang, K.-S. Chan, Z. H. Yuan, and H.-K. Lo, Phys. Rev. Lett. **131**, 110801 (2023).

[49] V. Zapatero, W. Y. Wang, and M. Curty, Quantum Sci. Technol. **8**, 025014 (2023).

[50] B. Qi, H. Gunther, P. G. Evans, B. P. Williams, R. M. Camacho, and N. A. Peters, Phys. Rev. Appl. **13**, 054065 (2020).

[51] B. Qi, P. G. Evans, and W. P. Grice, Phys. Rev. A **97**, 012317 (2018).

[52] P. Huang, T. Wang, R. Chen, P. Wang, Y. M. Zhou, and G. H. Zeng, New J. Phys. **23**, 113028 (2021).

[53] X. D. Wu, Y. J. Wang, Y. Guo, H. Zhong, and D. Huang, Phys. Rev. A **103**, 032604 (2021).

[54] C. Y. Li, C. Hu, W. Wang, R. Wang, and H.-K. Lo, arXiv: 2212.01876.

[55] Y. Tian, Y. Zhang, S. S. Liu, P. Wang, Z. G. Lu, X. Y. Wang, and Y. M. Li, Opt. Lett. **48**, 2953 (2023).

[56] H. Wang, Y. Li, Y. D. Pi, Y. Pan, Y. Shao, L. Ma, Y. C. Zhang, J. Yang, T. Zhang, W. Huang *et al.*, Commun. Phys. **5**, 162 (2022).

[57] Y. Pan, H. Wang, Y. Shao, Y. D. Pi, Y. Li, B. Liu, W. Huang, and B. J. Xu, Opt. Lett. **47**, 3307 (2022).

[58] L. C. Comandar, M. Lucamarini, B. Fröhlich, J. F. Dynes, Z. L. Yuan, and A. J. Shields, Opt. Express **24**, 17849 (2016).

[59] Z. L. Yuan, M. Lucamarini, J. F. Dynes, B. Fröhlich, M. B. Ward, and A. J. Shields, Phys. Rev. Appl. **2**, 064006 (2014).

[60] Z. L. Yuan, M. Lucamarini, J. F. Dynes, B. Fröhlich, A. Plews, and A. J. Shields, Appl. Phys. Lett. **104**, 261112 (2014).

[61] Z. L. Yuan, B. Fröhlich, M. Lucamarini, G. L. Roberts, J. F. Dynes, and A. J. Shields, Phys. Rev. X **6**, 031044 (2016).

[62] See Supplemental Material at http://link.aps.org/supplemental/10.1103/wgqv-cvr9 for results on heterodyne detections and data acquisition, calculation of the secret key rate, reverse reconciliation and privacy amplification, phase drift and scanning, comparison of the two ways to evaluate the secret key rate by numerical simulation, and performance comparison, which includes Refs. [7,9,18,47,48,50,52,55,56,58,63–69].

[63] J. Lin and N. Lütkenhaus, Phys. Rev. Appl. **14**, 064030 (2020).

[64] L. Xing, C. Zhou, J. Ma, Z. Chen, S. Yu, and X. Wang, Phys. Rev. Appl. **24**, 014018 (2025).

[65] S. S. Yang, Z. L. Bai, X. Y. Wang, and Y. M. Li, IEEE Photonics J. **9**, 1 (2017).

[66] S. Q. Ng, F. Kanitschar, G. Zhang, and C. Wang, arXiv: 2504.08298.

[67] A. A. E. Hajomer, F. Kanitschar, N. Jain, M. Hentschel, R. Zhang, N. Lütkenhaus, U. L. Andersen, C. Pacher, and T. Gehring, Light Sci. Appl. **14**, 255 (2025).
[68] M. Z. Wu, Y. Pan, J. H. Li, H. Wang, L. Fan, Y. Shao, Y. Li, W. Huang, S. Yu, B. J. Xu, and Y. C. Zhang, arXiv:2503.11431.
[69] H. Wang, Y. Li, T. Ye, L. Ma, Y. Pan, M. Z. Wu, J. H. Li, Y. M. Bian, Y. D. Pi *et al.*, Optica **12**, 1657 (2025).
[70] J. Lin, T. Upadhyaya, and N. Lütkenhaus, Phys. Rev. X **9**, 041064 (2019).
[71] A. Winick, N. Lütkenhaus, and P. J. Coles, Quantum **2**, 77 (2018).
[72] F. Kanitschar, I. George, J. Lin, T. Upadhyaya, and N. Lütkenhaus, PRX Quantum **4**, 040306 (2023).
[73] Y. Feng, R. H. Qiu, K. Zhang, X. Q. Jiang, M. X. Zhang, P. Huang, and G. H. Zeng, Sci. China Inf. Sci. **66**, 180511 (2023).
[74] Z. Lu, W. Liu, Y. Zhang, Z. Bai, and Y. Li, Phys. Rev. A **112**, 062613 (2025).